Table 1
Summary of the parameters for interfractional setup errors

	L-R			A-P			C-C		
	μ-INTER (Range, mm)	Σ-INTER (mm)	σ-INTER (mm)	μ-INTER (Range, mm)	Σ-INTER (mm)	σ-INTER (mm)	μ-INTER (Range, mm)	Σ-INTER (mm)	σ-INTER (mm)
Mandible	-0.2 (-2.8 to 4.1)	1.0	0.7	-0.1 (-3.0 to 2.4)	0.8	0.9	-0.2 (-2.4 to 3.0)	1.3	1.0
Maxilla	-0.7 (-3.5 to 2.3)	1.0	0.7	-0.1 (-2.3 to 1.5)	0.9	0.6	-0.5 (-4.2 to 1.8)	1.2	0.9
CV	-0.2 (-3.7 to 4.8)	0.9	1.6	-0.8 (-5.2 to 2.9)	0.8	1.2	0.8 (-3.2 to 4.5)	1.2	1.3
Skull base	NA	NA	NA	-0.6 (-2.8 to 1.9)	0.7	0.9	-0.4 (-4.3 to 2.0)	0.7	0.8

Abbreviations: L-R, left-right; A-P, anterior-posterior; C-C, cranio-caudal; CV, cervical vertebrae; NA, not applicable.

set-up errors were determined using the software in Somavision. In the present study, the intrafractional organ motions at each interval were defined as deviations of the coordinates of each landmark from those at the initial image taken at the start of the analysis. The systematic error of the organ motions for a specific patient, $Sp\text{-}intra$, is calculated as the mean of the organ motions evaluated six times for 15 min in the analysis of that patient. The mean of the $Sp\text{-}intra$ values for all the patients in a given population is denoted by $\mu\text{-}intra$, whereas its SD is given by $\Sigma\text{-}intra$. The random error of the organ motions for a specific patient, $\sigma p\text{-}intra$ was calculated as the SD of the intrafractional organ motions from interval to interval. To characterize the random errors of the organ motions in a given population, an appropriate average is by the root mean square of the $\sigma p\text{-}intra$ values for all the patients, and is denoted by $\sigma\text{-}intra$. The distribution of the intrafractional organ motions in a given population is characterized by the set ($\mu\text{-}intra$, $\Sigma\text{-}intra$, $\sigma\text{-}intra$).

Results

Interfractional setup errors and intrafractional organ motion errors

The values for the set of parameters ($\mu\text{-}INTER$, $\Sigma\text{-}INTER$, $\sigma\text{-}INTER$) and ($\mu\text{-}intra$, $\Sigma\text{-}intra$, $\sigma\text{-}intra$) measured for the four bony landmarks are shown in Tables 1 and 2, respectively. Since, deviations of the coordinates in the cranio-caudal direction were measured on both lateral and AP films, a larger deviation was adopted as a representative error for the bony landmarks. Positive values in the lateral, antero-posterior (AP), and cranio-caudal (CC) direction represent deviations in the right, cranial, and posterior direction of the patients. The mean of the systematic set-up errors ($\mu\text{-}INTER$) for all the landmarks ranged within 1 mm along all the coordinates. The distribution of the interfractional set-up errors of the mandible is shown graphically in Fig. 2. The SDs of the systematic set-up errors ($\Sigma\text{-}INTER$) distributed with a range of 0.7-1.3 mm. The average of the individual random set-up errors ($\sigma\text{-}INTER$) ranged from 0.7 to 1.6 mm.

As shown in Table 2, nine of eleven measured mean systematic errors for the intrafractional organ motions ($\mu\text{-}intra$) in all the directions ranged within 0.2 mm. The largest mean value of $\mu\text{-}intra$ was 0.4 mm in the AP direction of cervical vertebrae. Fig. 3 shows the distribution of the intrafractional organ motions of the mandible. The SDs of the systematic errors for the organ motions ($\Sigma\text{-}intra$) ranged within 1 mm (0.2-0.8 mm). The average of the individual random errors for the organ motions ($\sigma\text{-}intra$) ranged from 0.3 to 0.6 mm. In the present study, no significant differences in the magnitude of the interfractional set-up errors and intrafractional organ motions were observed among the four bony landmarks.

PTV- and PRV-margin

According to Stroom et al., the overall errors in a given patient group can be characterized by the overall distribution of systematic errors, $\Sigma - total = \sqrt{\Sigma - INTER^2 + \Sigma - intra^2}$, and the overall distribution of random errors,

Table 2
Summary of the parameters for intrafractional organ motion errors.

	L-R σ-intra (mm)	L-R Σ-intra (mm)	L-R μ-intra (Range, mm)	A-P σ-intra (mm)	A-P Σ-intra (mm)	A-P μ-intra (Range, mm)	C-C σ-intra (mm)	C-C Σ-intra (mm)	C-C μ-intra (Range, mm)
Mandible	0.3	0.3	0.1 (−0.7 to 1.2)	0.4	0.5	0.0 (−1.7 to 1.8)	0.6	0.8	−0.2 (−3.2 to 1.6)
Maxilla	0.6	0.7	0.1 (−1.9 to 3.0)	0.5	0.3	0.0 (−2.1 to 1.2)	0.5	0.5	0.0 (−1.8 to 1.7)
CV	0.4	0.7	−0.3 (−1.6 to 1.1)	0.5	0.8	0.4 (−0.9 to 3.5)	0.5	0.5	−0.2 (−1.6 to 1.7)
Skull base	NA	NA	NA	0.4	0.2	0.1 (−0.9 to 1.1)	0.5	0.6	0.1 (−1.4 to 2.1)

Abbreviations: L-R, left-right; A-P, anterior-posterior; C-C, cranio-caudal; CV, cervical vertebrae; NA, not applicable.

$\sigma - total = \sqrt{\sigma - INTER^2 + \sigma - intra^2}$, respectively [26]. Stroom et al. proposed an equation for the PTV margin [PTV-margin $= 2\Sigma$-total $+ 0.7\sigma$-total] [25]. The criterion was that more than 99% of the CTV should at least get 95% of the prescribed dose. McKenzie et al. proposed the recommended margin around the ORs, the planning organs at risk volume (PRV-margin). They proposed the equation [PRV-margin $= 1.3\Sigma + 0.5\sigma$] for serial ORs or small, parallel ORs [14]. The criterion was that the mean position of the edge of the ORs in any single direction would be completely encompassed by this margin in 90% of cases.

In the present study, the interfractional set-up errors and int afractional organ motions were analyzed in the different pa ient groups. Therefore, when Σ-total and σ-total values were calculated using the Σ-INTER, σ-INTER, Σ-intra, and σ-intra in the present study (Table 3), the obtained values did not strictly represent the overall distributions of the errors for the patient group of the head and neck tumors treated with IMRT at our department. However, both the groups were treated with IMRT using the same immobilizing system, and by the same treatment staffs, so the calculated PTV- and PRV-margins are clinically available for applying the appropriate margins to new patients with head and neck tumors treated with IMRT at our department. The calculated PTV- and PRV-margins using the equations by Stroom et al. and McKenzie et al. are shown in Table 4. The calculated PTV- and PRV-margins ranged from 2.0 to 3.6 mm and from 1.6 to 2.4 mm, respectively.

Discussion

When applying a new treatment technique including a new immobilization device or extending the indication of the technique to malignancies at other sites, one should analyze both the interfractional set-up errors and intrafractional organ motions in an initial group of patient ($n \approx 10$) for calculating the appropriate PTV margins [26]. However, in setting of the PTV-margins for head and neck tumors, the management of the organ motions is a subject of controversy. Gieleau et al. [6] claimed that the intrafractional organ motions of head and neck tumors could be neglected for calculating the PTV-margin since the values were trivial. Rosenthal et al. [22] analyzed the intrafractional organ motions of paranasal sinus carcinomas during a single fraction (approximately 16 min), and reported that the Σ-intra values (SDs of the systematic errors of the organ motions), ranged from 0.4 to 0.5 mm. The present study revealed that the Σ-intra values ranged from 0.2 to 0.8 mm during 15-min-treatment time. Although the SDs of the organ motions were revealed to be the sub-millimeter values in the present study, they should be taken account in calculating the PTV-margins in head and neck IMRT. IMRT commonly introduces relatively steep dose gradients around the PTV, and insufficient PTV-margins may yield the 'cold spot' in the CTV [8]. We combined the SDs of the set-up errors and organ motions, and showed that the PTV-margins ranged from 2.0 to 3.6 mm in head and neck IMRT. Since, no significant differences in the magnitude of the set-up errors and organ motions were observed among the four bony landmarks, a 5-mm margin was adopted as the PTV-margin for
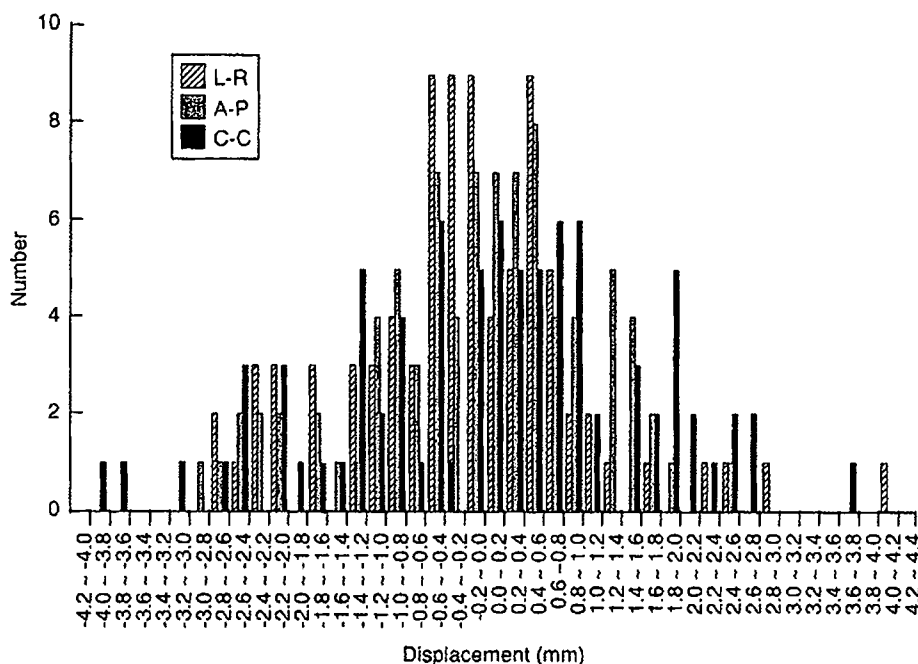
Fig. 2. The distribution of the interfractional set-up errors of the mandible. The displacements of the coordinate of the mandible between beam films and simulation films are plotted for the left-right (L-R) direction, anterior-posterior (A-P) direction, and cranio-caudal (C-C) direction.

tumors at any site in head and neck IMRT at our department, except tongue or laryngeal cancer, which is discussed later in this chapter.

With regard to the interfractional set-up errors, de Boer et al. reviewed three reports analyzing set-up errors in small patient groups ($n \approx 10$) with head and neck tumors, and

reported that the Σ-INTER and σ-INTER values ranged from 1.6 to 2.1 mm and from 1.0 to 2.0 mm, respectively [5]. In the present study, the Σ-INTER and σ-INTER values distributed with a range of 0.6-1.3 mm and 0.9-1.6 mm, respectively. Our results surpassed the values reviewed by de Boer et al. Hong et al. [8] reported the set-up errors for
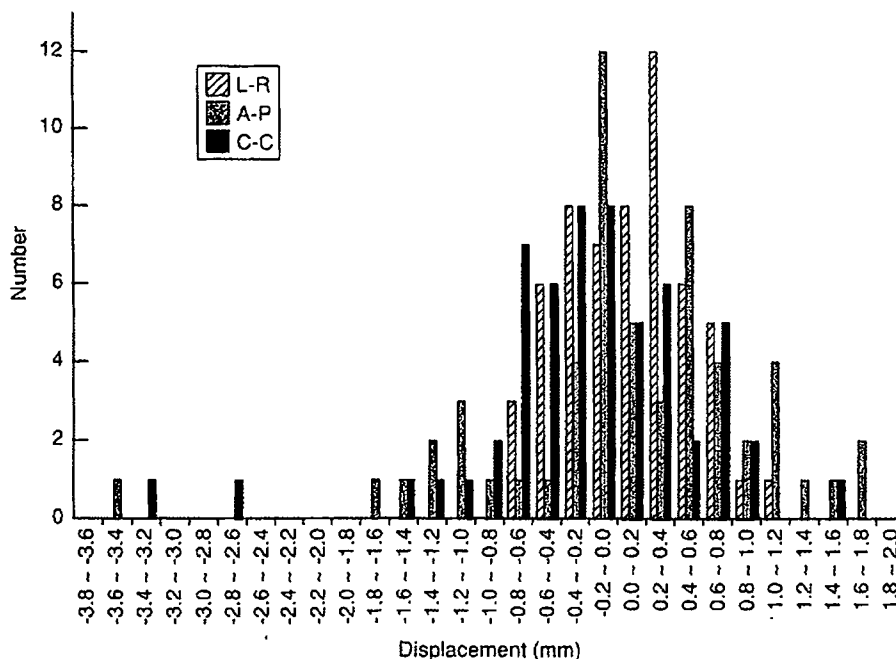

Fig. 3. The distribution of the intrafractional organ motion of the mandible. Two orthogonal films were digitally stored every 3 min for 15 min on the couch of the X-ray simulator under the same conditions as for the IMRT irradiation. The displacements of the coordinate of the mandible between the films taken every 3 min and initial film taken at the start of the analysis are plotted for the left-right (L-R) direction, anterior-posterior (A-P) direction, and cranio-caudal (C-C) direction.

Table 3
Summary of the total errors

	L-R		A-P		C-C	
	Σ-total (mm)	σ-total (mm)	Σ-total (mm)	σ-total (mm)	Σ-total (mm)	σ-total (mm)
Mandible	1.0	0.8	0.9	1.0	1.4	1.1
Maxilla	1.2	0.9	0.9	0.7	1.3	1.0
CV	1.1	1.6	1.1	1.3	1.3	1.4
Skull base	NA	NA	0.7	0.8	1.1	1.0

Abbreviations: L-R, left-right; A-P, anterior-posterior; C-C, cranio-caudal; CV, cervical vertebrae.

advanced head and neck tumors in 10 patients treated with conventional radiotherapy, in which all the patients were immobilized by conventional thermoplastic mask covering head and face. We calculated the Σ-INTER and σ-INTER values in the report by Hong et al. and found that they ranged from 2.7 to 4.0 mm and 2.3 to 2.8 mm, respectively. They incorporated these values in the IMRT treatment planning and reported that the substantial geometrical errors can lead to underdosing in the PTV and overdosing in the PRV. In the present study, we immobilized the patients with a thermoplastic shell covering head, neck and shoulder, which was fixed to the treatment couch. In some reports [6,7,20], a head, neck and shoulder immobilization shell, which is the same type as used in the present study, yielded smaller SDs of the set-up errors compared with a thermoplastic mask covering head and face alone. As concluded in the report by Hong et al. [8], rigorous immobilization devices such as the head, neck and shoulder immobilization shell may be prerequisite for highly conformal radiotherapy such as IMRT or 3D conformal radiotherapy for head and neck tumors. However, one should keep in mind that although the rigorous immobilization device and the sophisticated local infrastructure (treatment couch, linac laser beam system, etc.) are important factors for reproducibility of the patient positioning, experience and efforts of treatment stuffs including radiotherapists or nurses also depend on accuracy of the set-up [6,20]. Our extremely accuracy in the patient positioning may be in part attributable to zealous efforts of our treatment stuffs, such as adopting the strict criterion for couch position (less than 1 mm from the reference position), appropriate QA, or using a ink-soaked thin wire for depicting thin set up markers, etc.

Geometric uncertainties of ORs also have impacts on the dose distributions in Ors [11,16]. McKenzie et al. reported the recommended PRV-margin [14]. They proposed the equation [PRV-margin $= 1.3\Sigma + 0.5\sigma$] for serial ORs or small, parallel ORs. Since a dose higher than the tolerance dose for ORs comes broadly from a single direction of the high-dose region of an adjacent PTV, the equation of [PRV-margin $= 1.3\Sigma + 0.5\sigma$] is derived from a one-dimensional (1D) solution in calculating appropriate PRV-margin [14]. On the other hand, the boundaries of the CTV are potentially vulnerable to underdosing in all directions. A three-dimensional (3D) solution is required for calculating the appropriate PTV-margin. Since, use of the 3D solution leads to large values compared with the 1D solution, the PTV-margin is larger than the PRV-margin in general. One should keep in mind that if ORs are surrounded by the PTV in all

directions, the equation [PRV-margin $= 1.3\Sigma + 0.5\sigma$] should not be used for calculating the PRV-margin [14,30]. Since, in head and neck irradiation, salivary glands, spinal cord and brain stem are prone to be adjacent to the CTV, an appropriate setting of the PRV-margin is required for avoiding radiation injury of these ORs. The set-up errors and organ motions of four distinct bony landmarks estimated in the present study can be incorporated into the equation [PRV-margin $= 1.3\Sigma + 0.5\sigma$] for calculating the PRV-margins. The calculated PRV-margins distributed with a range of 1.8-2.4 mm. Therefore, 3-mm has been adopted as the PRV-margin at our department. However, no margins around parotid glands have been applied at our department [18], since the PRV-margins for the parotid glands reduce coverage of the nodal regions adjacent to the parotid glands as reported by Manning et al. [13].

In the present study, we analyzed the interfractional or intrafractional displacement of the four bony landmarks, not the treatment isocenter. The magnitudes of the interfractional and intrafractional errors were quantified by measuring the displacements of the coordinates of the four bony landmarks, which were determined relative to the isocenter. In published reports on analyses of the set-up errors, displacement of the isocenter on portal film or EPID from that on simulation films was measured by matching visible bony structures [1,5,6,20]. Since the maxilla, mandible and cervical spine can move independently with breathing or swallowing, interfractional or intrafractional displacement of these landmarks was expected to differ in magnitude. The dose of irradiation delivered to the PTV is determined by the position relative to the isocenter. Therefore, measuring the deviation of the coordinates of the bony landmarks relative to the isocenter is appropriate for analyzing set-up errors or organ motions in head and neck tumors, which are expected to move with underlying bone. The calculated

Table 4
Summary of the recommended PTV-margin and PRV-margin

	PTV-margin/PRV-margin		
	L-R (mm)	A-P (mm)	C-C (mm)
Mandible	2.7/1.8	2.5/1.7	3.6/2.4
Maxilla	3.0/2.0	2.4/1.6	3.2/2.1
CV	3.3/2.2	3.2/2.2	3.6/2.4
Skull base		2.0/1.3	2.8/1.9

Abbreviations: L-R, left-right; A-P, anterior-posterior; C-C, cranio-caudal; CV, cervical vertebrae.

PTV-margins in the present study, however, should not be applied to tongue or laryngeal tumors, the movement of which is independent of bone, since the organ motions of these tumors are large compared with the bony landmarks analyzed in the present study [29]. For analyses of the set-up errors or organ motions of these tumors, the use of implanted gold markers is helpful and feasible, as reported by van Asselen et al. [28].

We analyzed the intrafractional organ motions with a convenient and practical method. On the same couch of the X-ray simulator as the treatment couch has, the set-up procedure for IMRT was reproduced with the same immobilization device as used at the treatment, and intrafractional organ motions were monitored every 3 min for 15 min (6 times). EPID or a real time tracking system for radiopaque markers implanted within the tumors has been used for the analyses of the intrafractional organ motions [10,24,30]. However, the quality of the EPID is inadequate to analyze the errors in sub-millimeters. Although a real time tracking system is reliable for monitoring the position and movement of the PTV directly, the availability of this system is limited. Compared with these systems, our method is available at any institution without a sophisticated EPID or real time tracking system. In addition, our method may be able to reduce random errors of the intrafractional organ motions. By including the analysis of the organ motions in the preparation for head and neck IMRT, we can know the magnitude of the intrafractional organ motions for an individual patient before the start of the treatment, and reduce the organ motions by modifying the immobilization devise or educating the patient, if the magnitude of the organ motions is more than average at our department.

In conclusion, the calculated PTV-margin and PRV-margin distributed with a range of 2.0-3.6 mm and 1.8-2.4 mm, respectively. Therefore, we have adopted a 5-mm margin as the PTV-margin and 3-mm margin as the PRV-margin at our department for head and neck IMRT.

* Corresponding author. Minoru Suzuki, Radiation Oncology Research Laboratory, Research Reactor Institute, Kyoto University 2-1010, Asashiro-nishi, Kumatori-cho, Sennan gun, Osaka 590-0494, Japan. Tel.: +81 724 51 2390; fax: +81 724 51 2627. *E-mail address:* msuzuki@rri.kyoto-u.ac.jp

References

[1] Bel A, Keus R, Vijlbrief RE, Lebesque JV. Setup deviations in wedged pair irradiation of parotid gland andtonsillar tumors, measured with an electronic portal imaging device. Radiother Oncol 1995;37:153-9.

[2] Benedict SH, Cardinale RM, Wu Q, Zwicker RD, Broaddus WC, Mohan R. Intensity-modulated stereotactic radiosurgery using dynamic micro-multileaf collimation. Int J Radiat Oncol Biol Phys 2001;50:751-8.

[3] Bentel GC, Marks LB, Hendren K, Brizel DM. Comparison of two head and neck immobilization systems. Int J Radiat Oncol Biol Phys 1997;38:867-73.

[4] Cardinale RM, Benedict SH, Wu Q, Zwicker RD, Gaballa HE, Mohan R. A comparison of three stereotactic radiotherapy techniques; ARCS vs. noncoplanar fixed fields vs. intensity modulation. Int J Radiat Oncol Biol Phys 1998;42:431-6.

[5] de Boer HC, van Sörnsen de Koste JR, Creutzberg CL, Visser AG, Levendag PC, Heijmen BJ. Electronic portal image assisted reduction of systematic set-up errors in head and neck irradiation. Radiother Oncol 2001;61:299-308.

[6] Gilbeau L, Octave-Prignot M, Loncol T, Renard L, Scalliet P, Gregoire V. Comparison of setup accuracy of three different thermoplastic masks for the treatment of brain and head and neck tumors. Radiother Oncol 2001;58:155-62.

[7] Humphreys M, Guerrero Urbano MT, Mubata C, et al. Assessment of a customised immobilisation system for head and neck IMRT using electronic portal imaging. Radiother Oncol 2005;77: 39-44.

[8] Hong TS, Tomé WA, Chappell RJ, Chinnaiyan P, Mehta MP, Harari PM. The impact of daily setup variations on head-and-neck intensity-modulated radiation therapy. Int J Radiat Oncol Biol Phys 2005;61:779-88.

[9] Khoo VS, Oldham M, Adams EJ, Bedford JL, Webb S, Brada M. Comparison of intensity-modulated tomotherapy with stereotactically guided conformal radiotherapy for brain tumors. Int J Radiat Oncol Biol Phys 1999;45:415-25.

[10] Kitamura K, Shirato H, Seppenwoolde Y, et al. Three-dimensional intrafractional movement of prostate measured during real-time tumor-tracking radiotherapy in supine and prone treatment positions. Int J Radiat Oncol Biol Phys 2002; 53:1117-23.

[11] Kvinnsland Y, Muren LP. The impact of organ motion on intestine doses and complication probabilities in radiotherapy of bladder cancer. Radiother Oncol 2005;76:43-7.

[12] Lee N, Xia P, Quivey JM, et al. Intensity-modulated radiotherapy in the treatment of nasopharyngeal carcinoma: an update of the UCSF experience. Int J Radiat Oncol Biol Phys 2002;53:12-22.

[13] Manning MA, Wu Q, Cardinale RM, et al. The effect of setup uncertainty on normal tissue sparing with IMRT for head-and-neck cancer. Int J Radiat Oncol Biol Phys 2001;51:1400-9.

[14] McKenzie A, van Herk M, Mijnheer B. Margins for geometric uncertainty around organs at risk in radiotherapy. Radiother Oncol 2002;62:299-307.

[15] Mundt AJ, Lujan AE, Rotmensch J, et al. Intensity-modulated whole pelvic radiotherapy in women with gynecologic malignancies. Int J Radiat Oncol Biol Phys 2002;52:1330-7.

[16] Muren LP, Ekerold R, Kvinnsland Y, Karlsdottir A, Dahl O. On the use of margins for geometrical uncertainties around the rectum in radiotherapy planning. Radiother Oncol 2004;70:11-19.

[17] Muren LP, Smaaland R, Dahl O. Organ motion, set-up variation and treatment margins in radical radiotherapy of urinary bladder cancer. Radiother Oncol 2003;69:291-304.

[18] Nishimura Y, Nakamatsu K, Shibata T, et al. Importance of the initial volume of parotid glands in xerostomia for patients with head and neck cancers treated with IMRT. Jpn J Clin Oncol 2005;35:375-9.

[19] Pirzkall A, Carol M, Lohr F, Hoss A, Wannenmacher M, Debus J. Comparison of intensity-modulated radiotherapy with conventional conformal radiotherapy for complex-shaped tumors. Int J Radiat Oncol Biol Phys 2000;48:1371-80.

[20] Prisciandaro JI, Frechette CM, Herman MG, Brown PD, Garces YI, Foote RL. A methodology to determine margins by EPID measurements of patient setup variation and motion as applied to immobilization devices. Med Phys 2004;31: 2978-88.

[21] Remeijer P, Geerlof E, Ploeger L, Gilhuijs K, van Herk M, Lebesque JV. 3-D portal image analysis in clinical practice: an evaluation of 2-D and 3-D analysis techniques as applied to 30 prostate cancer patients. Int J Radiat Oncol Biol Phys 2000;46: 1281-90.

[22] Rosenthal SJ, Gall KP, Jackson M, Thornton Jr AF. A precision cranial immobilization system for conformal stereotactic fractionated radiation therapy. Int J Radiat Oncol Biol Phys 1995;33:1239-45.

[23] Saarilahti K, Kouri M, Collan J, et al. Intensity modulated radiotherapy for head and neck cancer: evidence for preserved salivary gland function. Radiother Oncol 2005;74: 251-8.

[24] Shimizu S, Shirato H, Ogura S, et al. Detection of lung tumor movement in real-time tumor-tracking radiotherapy. Int J Radiat Oncol Biol Phys 2001;51:304-10.

[25] Stroom JC, de Boer HC, Huizenga H, Visser AG. Inclusion of geometrical uncertainties in radiotherapy treatment planning by means of coverage probability. Int J Radiat Oncol Biol Phys 1999;43:905-19.

[26] Stroom JC, Heijmen BJM. Geometrical uncertainties, radio-therapy planning margins, and the ICRU-62 report. Radiother Oncol 2002;64:75-83.

[27] Suzuki M, Nakamatsu K, Kanamori S, et al. Feasibility study of the simultaneous integrated boost (SIB) method for malignant gliomas using intensity modulated radiotherapy (IMRT). Jpn J Clin Oncol 2003;33:271-7.

[28] van Asselen B, Dehnad H, Raaijmakers CP, Lagendijk JJ, Terhaard CH. Implanted gold markers for position verification during irradiation of head-and-neck cancers: a feasibility study. Int J Radiat Oncol Biol Phys 2004;59:1011-7.

[29] van Asselen B, Raaijmakers CP, Lagendijk JJ, Terhaard CH. Intrafraction motions of the larynx during radiotherapy. Int J Radiat Oncol Biol Phys 2003;56:384-90.

[30] van Herk M, Remeijer P, Rasch C, Lebesque JV. The probability of correct target dosage: dose-population histograms for deriving treatment margins in radiotherapy. Int J Radiat Oncol Biol Phys 2000;47:1121-35.

[31] Weltens C, Kesteloot K, Vandevelde G, Van den Bogaert W. Comparison of plastic and orfit® masks for patient head fixation during radiotherapy: precision and costs. Int J Radiat Oncol Biol Phys 1995;33:499-507.

[32] Zelefsy MJ, Fuks Z, Hunt M, et al. High-dose intensity modulated radiation therapy for prostate cancer: early toxicity and biochemical outcome in 772 patients. Int J Radiat Oncol Biol Phys 2002;53:1111-6.

Angled Forceps Used for Transbronchial Biopsy in Which Standard Forceps Are Difficult To Manipulate*

A Comparative Study

Shinji Sasada, MD; Yoshitaka Ogata, MD; Masashi Kobayashi, MD; Tomonori Hirashima, MD; Kunimitsu Kawahara, MD, PhD; Kaoru Matsui, MD; and Ichiro Kawase, MD

Objectives: To evaluate the usefulness of the Sasada transbronchial angled forceps (STAF) in patients with peripheral pulmonary lesions (PPLs), which are difficult to manipulate with standard forceps.

Methods: We have invented the STAF, a forceps with an angled tip. One hundred ten patients with PPLs that were difficult to reach with standard forceps were retrospectively evaluated. The patients first underwent bronchoscopy with a standard forceps and then with the STAF. The specimens obtained with standard forceps and those obtained with STAF were separately fixed and analyzed histologically. We compared the histologic diagnosis of the specimens obtained by STAF with that obtained by the specimens obtained with standard forceps. Statistical significance was calculated with the McNemar χ^2 statistic.

Results: The diagnostic yield of all lesions from the specimens obtained with STAF (86 of 110 lesions; 78.2%) was significantly higher than that of lesions from the specimens obtained with standard forceps (43 of 110 lesions; 39.1%; p < 0.001). Among malignant lesions, the yield obtained with STAF (60 of 72 lesions; 83.3%) was significantly higher than that obtained with standard forceps (32 of 72 lesions; 44.4%; p < 0.001). Among benign lesions, the yield obtained with STAF (26 of 38 lesions; 68.4%) was also significantly higher than that obtained with standard forceps (11 of 38 lesions; 28.9%; p < 0.001). Among the different lesion areas, the right upper lobe plus the left upper division gave the greatest difference in yield (STAF, 46 of 60 lesions; 76.7%; standard forceps, 22 of 60 lesions; 36.7%; p < 0.001). Among the different size ranges, the diagnostic yields obtained with STAF were significantly higher than that obtained with standard forceps except for the size range of ≤ 10 mm. There were two complications, pneumothorax and bronchial bleeding, both of which were controlled easily.

Conclusions: The STAF was shown to be useful for obtaining specimens that were sufficient for histologic diagnosis from PPLs that were difficult to manipulate with standard forceps.

(CHEST 2006; 129:725–733)

Key words: angled forceps; peripheral pulmonary lesions; transbronchial biopsy

Abbreviations: CS = curve-shaped; CTGNB = CT scan-guided needle biopsy; NSCLC = non-small cell lung cancer; PPL = peripheral pulmonary lesion; STAF = Sasada transbronchial angled forceps; TBB = transbronchial biopsy; VATS = video-assisted thoracic surgery

Since the 1970s, transbronchial biopsy (TBB) of the lung performed through a flexible broncho- scope has gained wide acceptance and has become the most common method of performing lung tissue biopsy.[1-4] The numbers of patients with peripheral pulmonary lesions (PPLs) have increased along with the incidence of lung adenocarcinoma.[5,6] Patients in whom a diagnosis cannot be made by flexible fiber- optic bronchoscopy need to undergo CT scan-guided needle biopsy (CTGNB) or video-assisted thoracic surgery (VATS).[7,8] However, CTGNB is associated with critical complications, including air embolism

422

and pleural dissemination.[9,10] On the other hand, in patients with poor performance status or in elderly patients, VATS is not always performed. Therefore, TBB with a flexible bronchoscope is still the recognized first-choice procedure used to diagnose PPLs. Nevertheless, we have experienced diagnostic failure with PPLs, even though PPLs can be visualized by radiographic fluoroscopy. With such lesions, conventional straight forceps are difficult to reach, and we cannot obtain a sufficient amount of material for histologic diagnosis. To solve this problem, we invented the Sasada transbronchial angled forceps (STAF). Our experience with 110 patients is reported in the present study.

MATERIALS AND METHODS

Patient Eligibility

We enrolled patients with PPLs that had been visualized by radiographic fluoroscopy and were difficult to manipulate by using standard forceps. Difficult-to-manipulate lesions presented in some situations as follows: the forceps could not really reach them, could hardly reach them, or could barely reach them. Such lesions were defined as *difficult PPLs*, and they mainly included solitary pulmonary lesions and mediastinum-involved tumors. Patients with diffuse pulmonary lesions or invasive shadows were excluded from the study. We judged the eligibility of the patient during bronchoscopy.

Study Design

The study was designed to retrospectively evaluate the usefulness of TBB with STAF in patients with difficult PPLs. Patients with difficult PPLs first underwent bronchoscopy with a standard forceps and then with STAF. The specimens obtained with standard forceps and those obtained with STAF were separately fixed and analyzed histologically. When either forceps absolutely could not reach a lesion that had been visualized by radiographic fluoroscopy, we did not perform a biopsy for safety reasons. Both specimens were diagnosed by two pathologists. We compared the histologic diagnosis obtained from the specimens by STAF with that from the specimens obtained by standard forceps. Cytologic and bacterial examinations were excluded in this study, because technical contamination was possible and could have caused misdiagnosis. Informed consent was obtained from all patients prior to undergoing the procedure.

*From the Departments of Thoracic Malignancy (Drs. Sasada, Kobayashi, Hirashima, and Matsui) and Pathology (Dr. Kawahara), Osaka Prefectural Medical Center for Respiratory and Allergic Diseases, Osaka, Japan; and the Department of Respiratory Medicine, Allergy and Rheumatic Diseases (Drs. Ogata and Kawase), Osaka University Graduate School of Medicine, Osaka, Japan.
Correspondence to: Shinji Sasada, Department of Thoracic Malignancy, Osaka Prefectural Medical Center for Respiratory and Allergic Disease, 3-7-1 Habikino, Habikino-Shi, Osaka 583-8588, Japan; e-mail: s-sasada@hbk.pref.osaka.jp

Equipment

We have invented a new forceps, called STAF (HBF-2010SH; Machida; Tokyo, Japan), that has an angled tip for obtaining adequate amounts of tissue from PPLs for histologic diagnosis. The structure of STAF is basically the same as that of standard forceps. STAF has a 12° angle 10 mm from the tip, so that the tip is perpendicular to the direction of the opening and shutting of the cup (Fig 1). STAF is a reusable product that can be fitted to any standard bronchoscope with channels having a diameter of ≥ 2.2 mm (eg, BF 1T-30, 40, or 1T-200, 240; Olympus; Tokyo, Japan). The cost is almost the same as that of standard forceps.

A New Biopsy Technique

To obtain adequate amounts of tissue for diagnosis, we invented a new biopsy technique called curve-shaped (CS) TBB. The CS-TBB method consists of five steps (Fig 2), which are clearly different from those of the conventional TBB method. First, we use standard forceps to identify the bronchus nearest to the lesion. Second, we switch to STAF and open the cup in front of the lesion. We search for a part of the lesion while letting the STAF turn and slide. Next, we make a CS motion by operating the bronchoscope, enabling a more perpendicular approach to the lesion. Finally, we push the forceps forward and perform the biopsy.

Statistical Analysis

The proportion of positive samples using STAF was compared with the proportion of positive samples using standard forceps. The patients who underwent bronchoscopy using STAF were exactly the same as those who underwent bronchoscopy using standard forceps. The statistical significance was calculated with the McNemar χ^2 statistic. A difference with a p value of < 0.05 was considered to be significant. The statistical analysis software was used for the analysis.

REPRESENTATIVE CASES

Case 1

A 25-year-old woman had a 23-mm lesion in the right upper lobe (Fig 3, *top, A*). Bronchoscopy was performed to confirm the diagnosis of the lesion. TBB with standard forceps failed to obtain specimens through the right B1a because the forceps could not reach the mass (Fig 3, *bottom left, B*). However, TBB with STAF succeeded in obtaining a sufficient amount of tissue for the specimens (Fig 3, *bottom right, C*), and the diagnosis of tuberculosis was histologically confirmed. The culture from the specimen was negative for tuberculosis.

Case 2

A 44-year-old man had a 30-mm lesion in the left lower lobe (Fig 4, *left, A*). Bronchoscopy was performed, and TBB performed with standard forceps failed to obtain specimens through the left B10e. However, TBB with performed STAF succeeded in obtaining a sufficient amount of tissue from the specimens to confirm a diagnosis of hamartoma (Fig 4, *right, B*).

Case 3

A 54-year-old man had a mediastinum-involved tumor in the left lung (Fig 5, *left, A*). Only STAF was able to reach the lesion
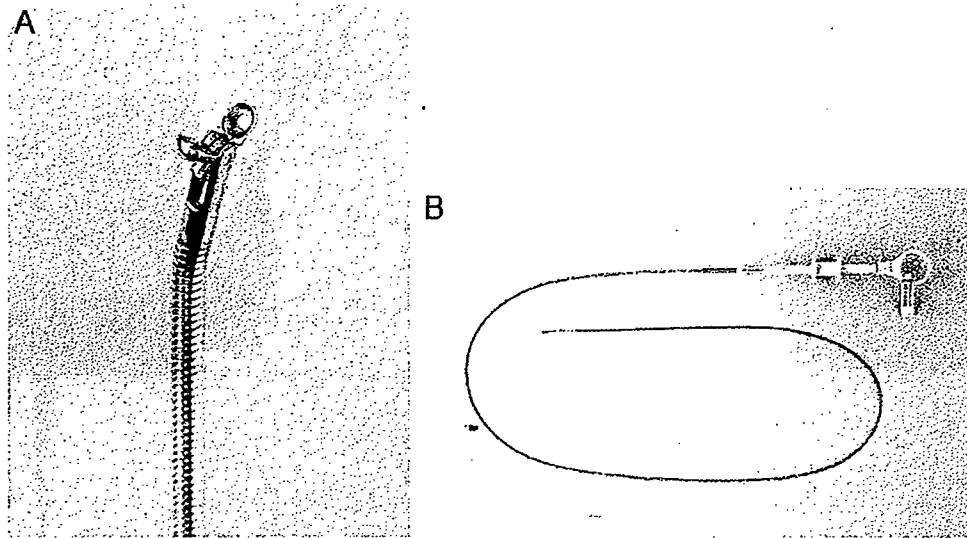
FIGURE 1. STAF. *Left, A:* Open position; the STAF has an angled tip. *Right, B:* the general shape of the STAF is almost the same as that of a standard forceps except for the angled tip.

(Fig 5, *right, B*), and a sufficient amount of tissue was obtained for the specimens to confirm a diagnosis of non-small cell lung cancer (NSCLC).

Case 4

A 74-year-old man had a 15-mm nodule in the right upper lobe (Fig 6, *top, A*). Specimens were obtained with standard forceps. and STAF through the right B3a. The specimens obtained with standard forceps revealed only a normal bronchial wall (Fig 6, *bottom left, B*); in contrast, the specimens obtained with STAF revealed adenocarcinoma (Fig 6, *bottom right, C*).

Case 5

A 34-year-old man had a 14-mm nodule in the right lower lobe (Fig 7, *top, A*). Specimens were obtained with standard forceps

and STAF through the right B6b. The specimens obtained with standard forceps were insufficient for pathological diagnosis, revealing only normal bronchial wall (Fig 7, *bottom left, B*). However, the specimens obtained with STAF revealed necrotizing epithelioid granuloma (Fig 7, *bottom right, C*), which suggested pulmonary tuberculosis. TBB with STAF succeeded in obtaining a specimen large enough for histologic examination.

RESULTS

One hundred ten consecutive patients with difficult PPLs who underwent bronchoscopy between August 2001 and July 2004 at the Osaka Prefectural Medical Center for Respiratory and Allergic Diseases were enrolled into the study. Of the 110
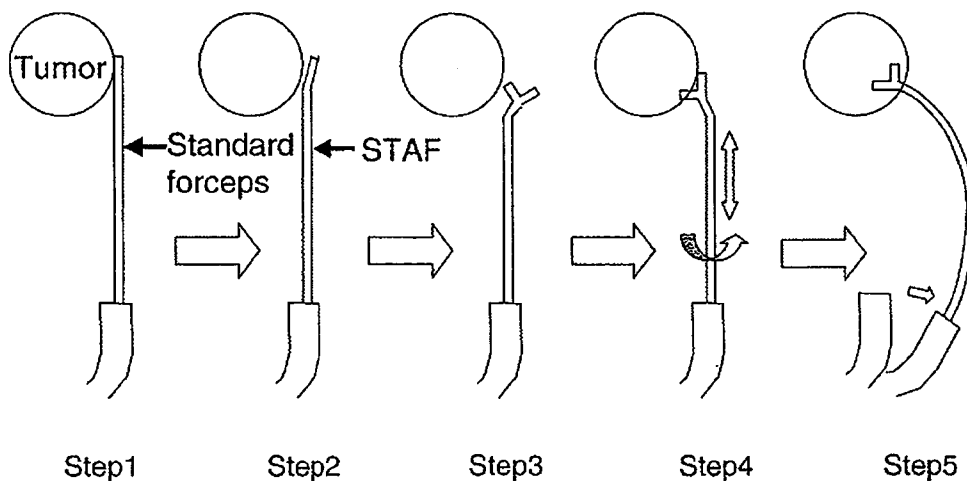

FIGURE 2. Method of performing CS-TBB. Step 1: search for the bronchus nearest to the lesion by using a standard forceps. Step 2: switch to STAF. Step 3: open the cup in front of the lesion. Step 4: turn and slide the STAF at the same time, and push forward. Step 5: make a CS motion by operating the bronchoscope, and obtain some tissue.
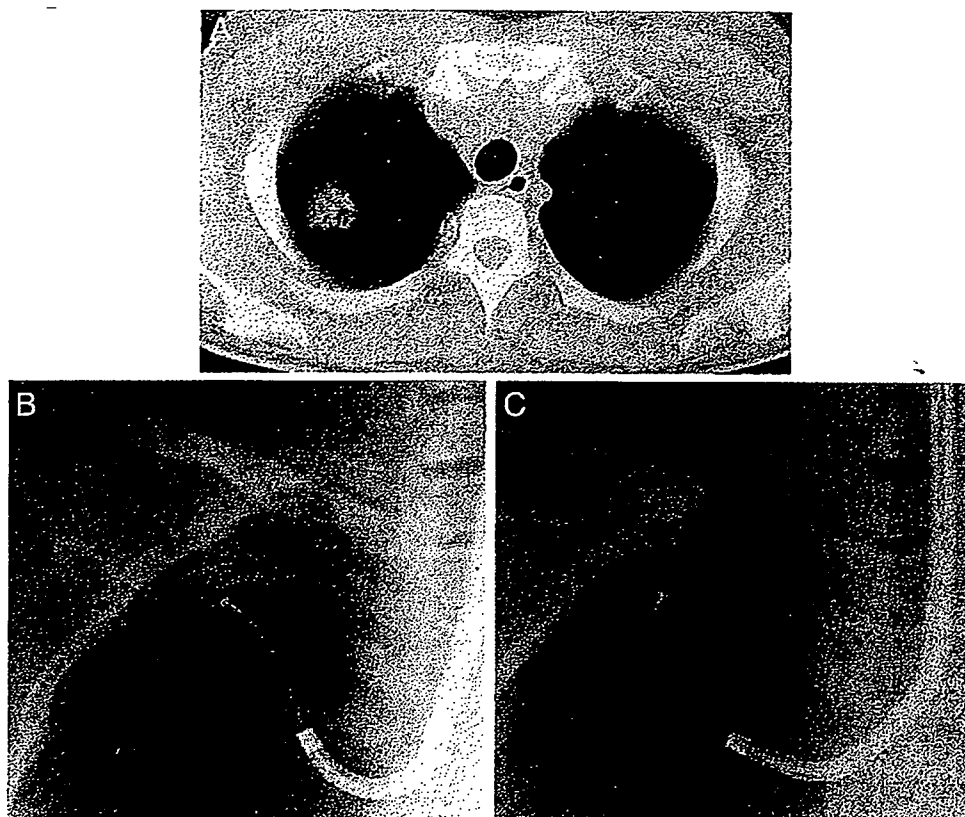
424

FIGURE 3. Case 1. A tuberculoma. *Top, A:* a chest CT scan reveals a coin lesion in the right upper lobe. *Bottom left, B:* a bronchoscopic image shows a standard forceps approaching a tumor through the right B1a. *Bottom right, C:* bronchoscopic image shows the STAF approaching the tumor. It forms a CS (*ie,* J-shape).

patients, 64 were men and 46 were women. The median age of the group was 67 (range, 25 to 86). The median size of the longest diameter of a lesion in the group was 20 mm (range, 6 to 60 mm). The longest diameters of all lesions revealed by chest CT scan were recorded.

Table 1 shows the diagnostic yields, and Table 2 shows the pathologic diagnoses in the 110 patients. The diagnostic yield of all lesions from the specimens obtained with STAF (86 of 110 lesions; 78.2%) was significantly higher than the that of lesions from the specimens obtained with standard forceps (43 of 110
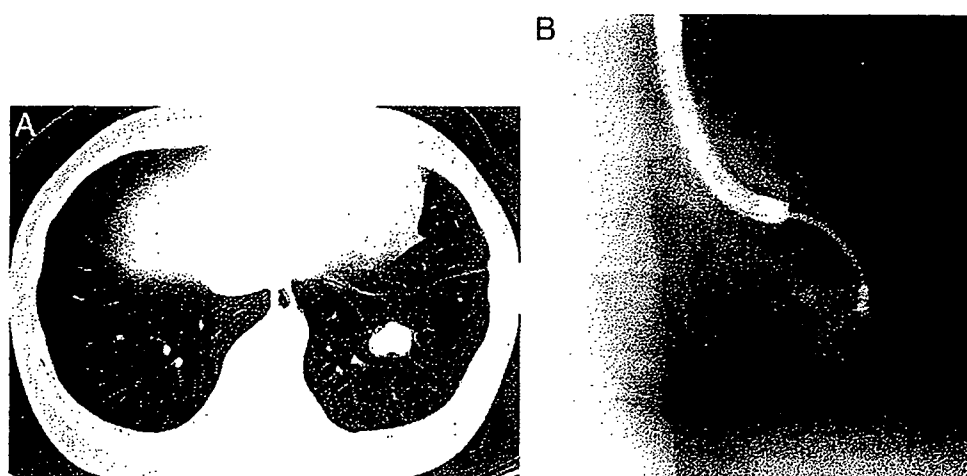

FIGURE 4. Case 2. A hamartoma. *Left, A:* a chest CT scan reveals a lesion in the left lower lobe. *Right, B:* a bronchoscopic image shows the STAF approaching a tumor through the left B10e. It forms a CS (*ie,* S-shape).
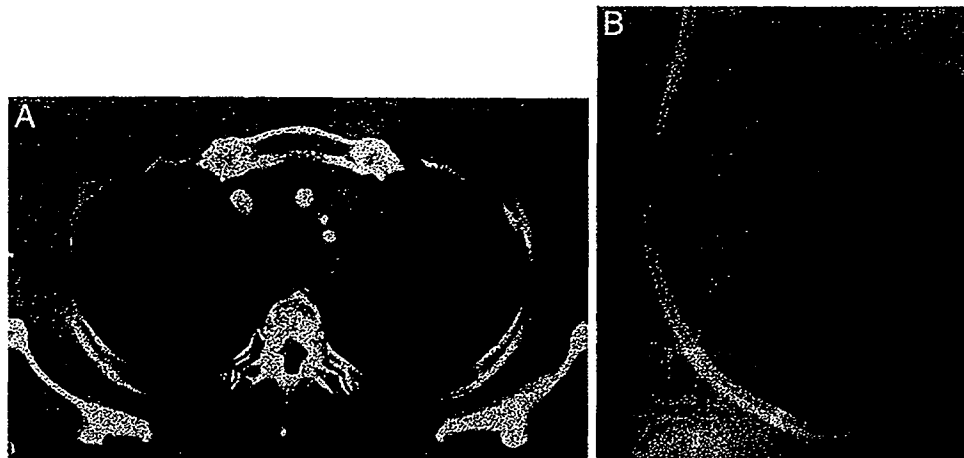
FIGURE 5. Case 3: NSCLC. *Left, A*: a chest CT scan reveals a mediastinum-involved tumor shadow on the left side. *Right, B*: a bronchoscopic image shows the STAF approaching the tumor through the left B3c.

lesions; 39.1%; $p < 0.001$). In malignant lesions, the yield obtained with STAF (60 of 72 lesions; 83.3%) was significantly higher than that obtained with standard forceps (32 of 72 lesions, 44.4%; $p < 0.001$). The pathologic diagnoses and the yields obtained with STAF included the following: adenocarcinoma, 86% (43 of 50 lesions); squamous cell carcinoma, 90% (9 of 10 lesions); small cell carcinoma, 100% (2 of 2 lesions); undifferentiated carcinoma, 80% (4 of 5 lesions); metastasis, 50% (2 of 4 lesions); and carcinoid tumor, 0% (0 of 1 lesion). In benign lesions, the yield obtained with STAF (26 of 38 lesions; 68.4%) was significantly higher than that obtained with standard forceps (11 of 38 lesions;
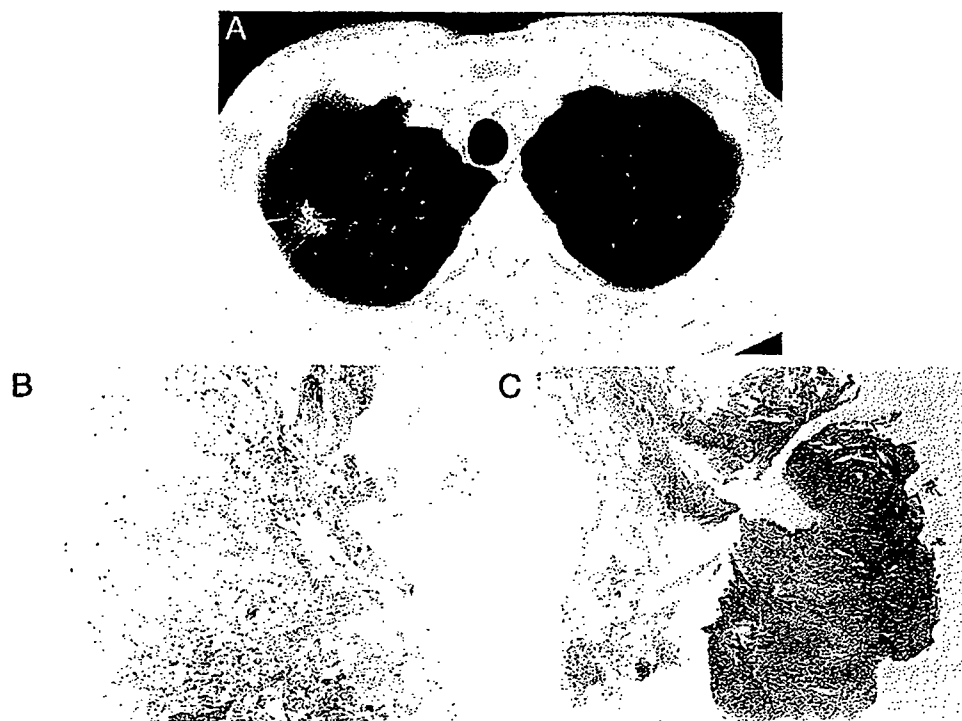

FIGURE 6. Case 4: a lung adenocarcinoma. *Top, A*: a chest CT scan reveals a coin lesion in the right upper lobe. *Bottom left, B*: the biopsy specimen obtained with standard forceps through the right B3a reveals only normal bronchial wall (hematoxylin-eosin, original ×40). *Bottom right, C*: STAF biopsy specimen reveals adenocarcinoma (hematoxylin-eosin, original ×40).
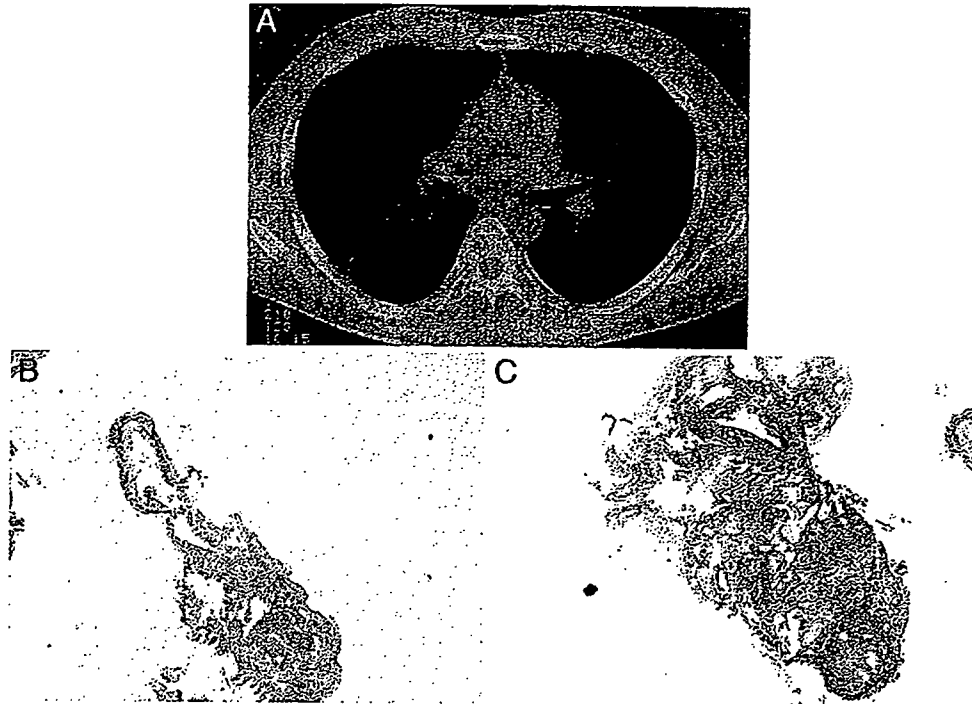
FIGURE 7. Case 5: a tuberculoma. *Top, A:* a chest CT scan reveals a coin lesion in the right lower lobe. *Bottom left, B:* the biopsy specimen obtained with standard forceps through the right B6b reveals a normal bronchial wall (hematoxylin-eosin, original ×40). *Bottom right, C:* STAF biopsy specimen reveals necrotizing epithelioid granuloma (hematoxylin-eosin, original ×40).

28.9%; $p < 0.001$). The diagnoses and yields obtained with STAF included the following: nonspecific inflammation, 57.1% (8 of 14 lesions); mycobacteriosis, 77.8% (7 of 9 lesions); hamartoma, 50% (4 of 8 lesions); organizing pneumonia, 100% (4 of 4 lesions); cryptococcosis, 100% (2 of 2 lesions); and lung abscess, 100% (1 of 1 lesion). Three patients underwent a second bronchoscopy when the first procedure failed to yield a specific diagnosis. Two of the specimens obtained in the second bronchoscopy resulted in a diagnosis.

Table 3 shows the diagnostic yield for each lesion area. Among the different lesion areas, the right upper lobe plus the left upper division gave the greatest difference in yield (STAF, 46 of 60 lesions

[76.7%]; standard forceps, 22 of 60 lesions [36.7%]; $p < 0.001$). Table 4 shows the diagnostic yield for each size range. Among the different size ranges, the diagnostic yields obtained with STAF were significantly higher than that obtained with standard forceps except for those with a size of ≤ 10 mm.

Of 24 patients in whom a diagnosis could not be established, 11 were operated on. Diagnosis was

Table 1—*Diagnostic Yields From PPLs Biopsied With STAF and Standard Forceps*

Variables	STAF		Standard Forceps		
	No./Total No.	%	No./Total No.	%	p Value*
Positive sample	86/110	78.2	43/110	39.1	< 0.001
Malignant	60/72	83.3	32/72	44.4	< 0.001
Benign	26/38	68.4	11/38	28.9	< 0.001

*By McNemar test.

Table 2—*Clinical Diagnosis of PPLsin 110 Patients Who Underwent Bronchoscopy With STAF*

Lesions	No./Total No. (%)
Malignant	
Adenocarcinoma	43/50 (86)
Squamous cell carcinoma	9/10 (90)
Small cell carcinoma	2/2 (100)
Undifferentiated carcinoma	4/5 (80)
Metastasis	2/4 (50)
Carcinoid	0/1 (0)
Total	60/72 (83.3)
Benign	
Nonspecific inflammation	8/14 (57.1)
Mycobacteriosis	7/9 (77.8)
Hamartoma	4/8 (50)
Organizing pneumonia	4/4 (100)
Cryptococcosis	2/2 (100)
Lung abscess	1/1 (100)
Total	26/38 (68.4)

Table 3—*Effect of Lesion Area on Diagnostic Yield of PPLs Obtained With STAF and Standard Forceps**

	STAF		Standard Forceps		
Lesion Area	No./Total No.	%	No./Total No.	%	p Value†
RUL + LUD	46/60	76.7	22/60	36.7	< 0.001
RML + Lingula	13/17	76.5	5/17	29.4	0.004
Lower superior (B6)	10/11	90.9	4/11	36.4	0.014
Lower basal	17/22	77.3	12/22	54.5	0.025

*RUL = right upper lobe; LUD = left upper division; RML = right middle lobe.
†By McNemar test.

made by transbronchial needle aspiration in two further patients. In 1 patient diagnosis was made by transcutaneous needle biopsy, and in 10 further patients it was made by serial observations. There were two complications (pneumothorax and bronchial bleeding), both of which were controlled easily.

DISCUSSION

Flexible fiberoptic bronchoscopy is routinely used for the diagnosis of PPLs. Flexible fiberoptic bronchoscopy in conjunction with TBB, bronchial brushing, or bronchial washing cytology has given physicians an additional procedure to aid in diagnosis. In patients with peripheral lung cancer, transbronchial needle aspiration has been developed.[11,12] However, benign pulmonary lesions are not usually diagnosed by cytologic examination, and thus lung resections are ultimately needed. Active tissue biopsy is required for the improvement of the diagnostic efficiency of PPLs, including benign lesions.

We had a patient in whom a critical air embolism developed during CTGNB, and we were thus confronted with the necessity of developing a new diagnostic procedure. We considered that the follow-

Table 4—*Effect of Lesion Size on Diagnostic Yield of PPLs Obtained With STAF and Standard Forceps**

	STAF		Standard Forceps		
Lesion Size, mm	No./Total No.	%	No./Total No.	%	p Value†
≤ 10	2/7	28.6	2/7	28.6	NS
> 10 to ≤ 20	39/49	79.6	17/49	34.7	< 0.001
< gt>20 to ≤ 30	28/31	90.3	16/31	51.6	< 0.001
> 30	17/23	73.9	8/23	34.8	0.002

*NS = not significant.
†By McNemar test.

ing three conditions are required in a new method. The first is that it must be safe for the patient and the staff. The second is that it should be inexpensive and easily introduced into many institutions. The final condition is that it is able to obtain specimens that can be used to histologically diagnose even benign lesions. Therefore, to satisfy these requirements, we should approach a lesion more perpendicularly by a standard bronchoscope to improve tissue collection.

We invented STAF as a new device for diagnosis to be used with a standard bronchoscope (Fig 1). STAF has a 12° angle 10 mm from the tip, and this structure was the most controllable in our experience. If the tip angle is ≤ 10°, the forceps cannot grasp the edge of the lesion. On the other hand, if the tip angle is > 15°, the forceps flexes too much during the approach. We also invented a new biopsy technique to control STAF more effectively (Fig 2). The CS-TBB method enables a perpendicular approach. The slight angle of the tip, the flexural direction perpendicular to the opening, and the shutting of the cup are necessary conditions to make a CS motion successfully. The CS-TBB method has two typical approach patterns, called the *J-shape* (Figs 3, bottom right, *C*, and 5, right, *B*) and the *S-shape* (Fig 4, right, *B*) in bronchoscopic images. These approach patterns are thought to be very effective for obtaining specimens from PPLs, because we can apply force directly to the lesion.

In this study, the diagnostic yield from the malignant lesions obtained with STAF was 83.3%. This result is thought to be almost the same as or greater than that obtained in patients with PPLs, counting what a standard forceps can easily reach.[13,14] Previous studies[15,16] have reported that the diagnostic yields in peripheral pulmonary benign lesions were 50 to 65.8%. In the present study, the diagnostic yield obtained with STAF was 84.6%. This result is significantly higher than that obtained in previous studies. In the diagnostic analysis of lesions in each area of the lung (Table 3), the STAF was often used to obtain a specimen from a lesion in the right upper lobe and the left upper division. This reflects the fact that the upper lobe is difficult to reach anatomically. STAF was found to be effective for obtaining specimens form these lesions. In the diagnostic analysis of each size range (Table 4), efficacy was poor for lesions < 10 mm, which cannot be clearly visualized by radiographic fluoroscopy. STAF is thought to be effective for use with all lesions that can be visualized by radiographic fluoroscopy. Using the STAF, the lesion can be visualized by radiographic fluoroscopy; it seems that using STAF has a benefit even if it is any difficult area.

There are three principal reasons why the diagnostic yield from TBB specimens obtained with

STAF was superior to that from specimens obtained with standard forceps. First, STAF was able to approach the lesion after being advanced into the bronchus of choice by flexure of the tip. Second, STAF was able to grasp the lesion well by a more perpendicular application of the conventional biopsy method. Third, STAF was able to obtain enough tissue for histologic examination. STAF also has some original applications. In patients with a mediastinum-involved tumor that a standard forceps cannot really reach, STAF easily reaches the lesion and can obtain sufficient material for histological examination. STAF is also useful for benign tumors or metastatic lesions, which communicate poorly with the bronchi. In these lesions, we expect that STAF can break a surrounding bronchial wall and grasp a lesion. We think that these types of lesions are most effectively approached using the STAF. To obtain further effects, several variations of a product are essential, such as shaft flexibility, flexure angle of the tip, and shape of the cup.

The complications from TBB performed with STAF, such as bronchial bleeding and pneumothorax, were mostly mild. These were similar to those from conventional TBB. We think that this is because our new method is basically conventional bronchoscopy performed with a new device and a new technique. But a carelessly performed operation could cause critical complications; for example, the rupture of great vessels due to approaching adjacent mediastinal lesions. In addition, if the channel of the bronchoscope is ≤ 2 mm in diameter, a careless operation may cause fiber damage. The use of bronchoscopes with a channel diameter of > 2.2 mm is preferable.

CTGNB and VATS have been performed worldwide.[7,8] But CTGNB is considered to be more invasive than TBB because of the possibility of critical complications, including air embolism and pleural dissemination,[9,10] while VATS is not always performed in patients with poor performance status or in the elderly. Other transbronchial diagnostic procedures include bronchoscopy with an ultrathin bronchoscope coupled with virtual navigation,[17] and endobronchial ultrasonography-guided TBB.[18] But these procedures involve complicated methods and are not yet widely used. Widely used diagnostic procedures should be safe and easy to use. When we compare our new diagnostic procedure with other diagnostic procedures, we find that its safety characteristics are superior to those of CTGNB and VATS, while its ease of operation is superior to that of the ultrathin bronchoscope with virtual navigation and endobronchial ultrasonography-guided TBB. Furthermore, we do not require a new investment because the cost is almost the same as that of

standard forceps. Consequently, from the point of view of safety, ease of operation, and cost-effectiveness, STAF can be used in any patients at any institution. However, physicians must learn and understand this biopsy technique well, and training is necessary.

In some studies,[19,20] a subgroup of patients with NSCLC have had specific mutations in the epidermal growth factor receptor gene that correlated with clinical responsiveness to the tyrosine kinase inhibitor gefitinib. But the accuracy of histologic diagnosis of peripheral lung cancer with TBB specimens is not always sufficient. We achieved a superior accuracy of histologic diagnosis in peripheral lung cancer (89.5%) between April 2002 and March 2003, and it was thought to be an additive effect of the innovation of STAF. Successful TBB with a low risk of severe complications is also important for predicting the efficacy of target therapies, because such information requires repeated biopsies. The adequate TBB specimens that were obtained with STAF are expected to contribute to the performance of gene analysis in patients with NSCLC in the future.

Conclusions

STAF was shown to be useful for obtaining sufficient specimens for histologic diagnosis from PPLs, which are difficult to manipulate with standard forceps, and the use of STAF resulted in a significant improvement in the diagnostic efficiency of TBB. CS-TBB performed with STAF can provide a high accuracy with safety and ease, so that this new device and technique may become widespread.

References

1 Zavala DC. Diagnostic fiberoptic bronchoscopy: techniques and results of biopsy in 600 patients. Chest 1975; 68:12–19
2 Mitchell DM, Emerson CJ, Collins JV, et al. Transbronchial lung biopsy with the fiberoptic bronchoscope: analysis of results in 433 patients. Br J Dis Chest 1981; 75:258–262
3 Smith CW, Murray GF, Wilcox BR, et al. The role of transbronchial lung biopsy in diffuse pulmonary disease. Ann Thorac Surg 1977; 24:54–58
4 Chopra SK, Ben-Isaac F. Transbronchial lung biopsy using fiberoptic bronchoscope. South Med J 1977; 70:302–304
5 Travis WD, Travis LB, Devesa SS. Lung cancer. Cancer 1995; 75(suppl):191–202
6 Barsky SH, Cameron R, Osann KE, et al. Rising incidence of bronchioloalveolar lung carcinoma and its unique clinicopathologic features. Cancer 1994; 73:1163–1170
7 Tsukada H, Satou T, Iwashima A, et al. Diagnostic accuracy of CT-guided automated needle biopsy of lung nodules. AJR Am J Roentgenol 2000; 175:239–243
8 Savage C, Morrison RJ, Zwishenberger JB. Bronchoscopic

429

diagnosis and staging of lung cancer. Chest Surg Clin N Am 2001; 11:701–721

9 Aberle DR, Gamsu G, Golden JA. Fetal systemic arterial air embolism following lung needle aspiration. Radiology 1987; 165:351–353

10 Seyfer AE, Walsh DS, Graeber GM, et al. Chest wall implantation of lung cancer after thin-needle aspiration biopsy. Ann Thorac Surg 1989; 48:284–286

11 Kawaraya M, Gemba K, Ueoka H, et al. Evaluation of various cytological examinations by bronchoscopy in the diagnosis of peripheral lung cancer. Br J Cancer 2003; 89:1885–1888

12 Baba M, Iyoda A, Yasufuku K, et al. Preoperative cytodiagnosis of very small-sized peripheral-type primary lung cancer. Lung Cancer 2002; 37:277–280

13 Kusunoki Y, Takifuji N, Takada M, et al. Transbronchial tumor biopsy (TBTB) during fibreoptic bronchoscopy in the diagnosis of peripheral lung disease. J Jpn Soc Bronchol 1991; 13(suppl):92–97

14 Ichinose Y, Yonemaru M, Yamasawa H, et al. The combination of bronchoscopic curettage and broncho-alveolar lavage for the diagnosis of peripheral solitary shadows on chest X-ray films. J Jpn Soc Bronchol 1991; 13:235–241

15 Chechani V. Bronchoscopic diagnosis of solitary pulmonary nodules and lung masses in the absence of endobronchial abnormality. Chest 1996; 109:620–625

16 Nakata M, Kimura K, Hojyo T, et al. Transbronchial biopsy for peripheral lung lesions. J Jpn Soc Bronchol 1997; 19:379–382

17 Asano F, Matsuno Y, Matsushita T, et al. Transbronchial diagnosis of a pulmonary peripheral small lesion using an ultrathin bronchoscope with virtual bronchoscopic navigation. J Bronchol 2002; 9:108–111

18 Kurimoto N, Miyazawa T, Okimasa S, et al. Endobronchial ultrasonography using a guide sheath increases the ability to diagnose peripheral pulmonary lesions endoscopically. Chest 2004; 126:959–965

19 Lynch TJ, Bell DW, Sordella R, et al. Activating mutations in the epidermal growth factor receptor underlying responsiveness of non-small cell lung cancer to gefitinib. N Engl J Med 2004; 350:29–39

20 Paez JG, Janne PA, Lee JC, et al. EGFR mutations in lung cancer: Correlation with clinical response to gefitinib therapy. Science 2004; 304:1497–1500

430

Characterization of preexisting humoral immunity specific for two cancer-testis antigens overexpressed at the mRNA level in non-small cell lung cancer

Yoshihiro Watanabe[1]*, Stephen LePage[1], Mark Elliott[1], Heather Secrist[1], Takao Tanaka[2], Masaaki Kawahara[2], Akihide Matsumura[2], Shigeto Hosoe[2], Mitsumasa Ogawara[2], Masaji Okada[2], Betsey Repasky[3], Paul Sleath[1], Tongtong Wang[1], and Robert Henderson[1]

[1]Department of Immunology and Antigen Discovery of Corixa Corporation, 1124 Columbia Street, Seattle, WA 98104, USA
[2]National Kinki-Chuo Hospital for Chest Diseases, Sakai, Japan
[3]Roswell Park Research Institute, Buffalo, NY 14263, USA
*Current address: Biological/Pharmacological Research Laboratories, Japan Tobacco Inc., 1-11-1 Murasaki-cho, Takatsuki, Osaka 569-1125, Japan

Keywords: human, non-small cell lung cancer, tumor antigens, L514S, L552S, humoral immunity, epitope mapping

In order to establish a rationale for immunotherapy for lung cancer, we have investigated immunological characteristics of tumor-associated antigens (TAAs) discovered through molecular approaches. Preexisting Abs specific to these predicted TAAs were examined using specimens of lung pleural effusions (LPEs) and sera in non-small cell lung cancer (NSCLC) patients. The novel cancer-testis (CT) antigens L514S and L552S were highly expressed in approximately half of the NSCLC tissues and established cell lines examined. When lung cancer patients in the USA and Japan were screened, 13%, 17%, and 5% were found to have Abs specific to recombinant L514S, L552S, and NY-ESO-1 proteins, respectively, whereas 48 normal donors had no Abs to these three CT antigens. The Ab titers specific to recombinant L552S and L514S proteins were similar to, and slightly lower than, Abs specific to NY-ESO-1 in stage IV NSCLC patients. To further characterize the preexisting specific Abs, the epitopes were analyzed using 20-aa length peptides entirely covering both antigens. An epitope common to the patients' L514S-specific Abs was identified as aa 85-100 and multiple epitopes, including a major epitope (aa 141-160), were identified for L552S-specific Abs. The Ab epitopes thus identified are not found in human, animal, or bacterial proteins, other than L514S, L552S, or XAGE-1. These data clearly demonstrate that both molecularly defined CT antigens L514S and L552S are immunogenic, at least in terms of humoral responses, suggesting that both CT antigens are promising candidates for immunotherapy.

Introduction

Immunotherapy using cytokines and identified TAAs can achieve certain benefits for melanoma patients, as suggested by our accumulated immunological knowledge of TAAs (1). However, it is not yet clear that immunotherapy can be applied to patients with other forms of cancer, nor is it known which TAAs are best suited to cancers such as lung cancer. Preexisting immunity in patients is proof of the immunogenicity of TAAs and can be dramatically enhanced by vaccination (2, 3). Studies have been undertaken in order to discover novel immunogenic TAAs and to ascertain how widely these TAAs are recognized by cancer patients. These TAAs have been categorized as follows: (i) CT antigens (4, 5, 6); (ii) oncofetal antigens (7, 8); (iii) overexpressed differentiation antigens (9, 10); and (iv) mutated antigens (11, 12). Recently, much attention has been devoted to

CT antigens as they are highly expressed in a wide variety of tumors and include potent immunogenic TAAs such as MAGE, GAGE, NY-ESO-1/CT6.1, and others (4, 5, 6, 13, 14).

Our study attempts to use molecular methods to identify novel tumor-specific antigens in NSCLC patients. A couple of these TAAs had been previously classified as CT antigens by molecular characterization (15). Following that, we studied the preexisting immunity and characteristics of these CT antigens by assessing how widely and strongly they are recognized in lung cancer patients. L514S is a novel antigen expressed in cancer and in normal testis tissues at the mRNA level. L552S is a CT antigen located on the X chromosome that is an alternatively spliced form of XAGE-1/CT12.1 (16). It has already been determined that the mRNA expression of these antigens is high in NSCLC patients. These CT antigens were examined in conjunction with NY-ESO-1, the well-known CT antigen frequently associated with both humoral and cellular immune responses (5, 17, 18, 19). L514S and L552S were recognized by multiple specimens in a fashion similar to that of NY-ESO-1. Epitope analysis of the patients' specific Abs also identified a couple of major epitopes in L514S and L552S. The homology search that followed confirmed that the amino acid sequences of major epitopic peptides are fully specific to L514S, L552S, or XAGE-1.

These data show that L514S and L552S induced specific Abs, as can be seen from the titer of the antibodies detected in NSCLC patients. A comparable analysis using the known CT antigen NY-ESO-1 showed that L514S and L552S are both immunogenic and are promising candidates for immunotherapeutic, as well as diagnostic, use.

Results

Molecular characterization of lung cancer antigens

L514S is an NSCLC-specific antigen that was discovered by the cDNA-subtraction method (15), although a detailed analysis of how frequently lung cancer specimens express this antigen has not been conducted. Real-time PCR analyses were set up, and Figure 1 shows representative data for L514S in the lung

squamous cell carcinoma panel. Eleven of twenty squamous cell carcinomas highly expressed L514S mRNA, and 40% of adenocarcinomas were also positive (data not shown), while normal tissues and cells other than the testis were negative for its expression. In Table 1, we summarize the mRNA expression of the three different antigens - L514S, L552S, and NY-ESO-1 - in NSCLC. About 40% of NSCLCs and more than half of the lung adenocarcinomas specimens examined highly express L552S (5, 16). NY-ESO-1 mRNA expression was observed in 12% of our adenocarcinoma panel; this frequency is similar to those reported earlier for NSCLC (17, 20).

Preexistence of Abs specific to NSCLC antigens in patients

First, the antibody responses to L514S and L552S in lung cancer patients' sera and in pleural effusions of NSCLC were examined. A total of 40 pleural effusions collected from advanced stage NSCLC patients (stage IV) were set up to analyze Abs specific to both recombinant CT antigens. Recombinant NY-ESO-1 protein was set up in parallel, as a control antigen. Pleural effusions that had Abs specific to L514S and L552S by ELISA were confirmed by Western blot analysis. Interestingly, several NSCLC patients whose pleural effusions had Abs specific to L514S, L552S, and/or NY-ESO-1 were identified. Representative data are shown in Figure 2A. Pleural effusion 659-23 had Abs specific to recombinant L514S, which had the expected molecular weight of 16 kDa. The Western blot band corresponding to recombinant L514S did not disappear when E. coli lysate was added (data not shown). This appears to confirm that detectable Ab responses were not specific to contaminated E. coli proteins, since recombinant proteins were derived from E. coli and patients frequently had strong Abs specific to E. coli proteins. Pleural effusion 298-19 had Abs specific to L514S with

low intensity, and to L552S with high intensity. Pleural effusion 574-57 had Abs specific to NY-ESO-1. In contrast, 6 pleural effusions of subjects without cancer had no Abs specific to these CT antigens, including NY-ESO-1 (data not shown).

Antibodies to these CT antigens were also found in the sera of multiple NSCLC patients. In Figure 2B, the results of Western blot analysis are shown for each CT antigen. The bands in the Western blot did not disappear even when E. coli lysate was added. Moreover, the same patient's pleural effusion and serum had Abs specific to the same cancer antigens. For example, L552S-specific Abs were detected in both the pleural effusion and the serum of one patient (data not shown). These results indicate that these three antigens are immunogenic in terms of humoral responses detected by Western blot analyses, and that the Abs detected were specific to individual CT antigens.
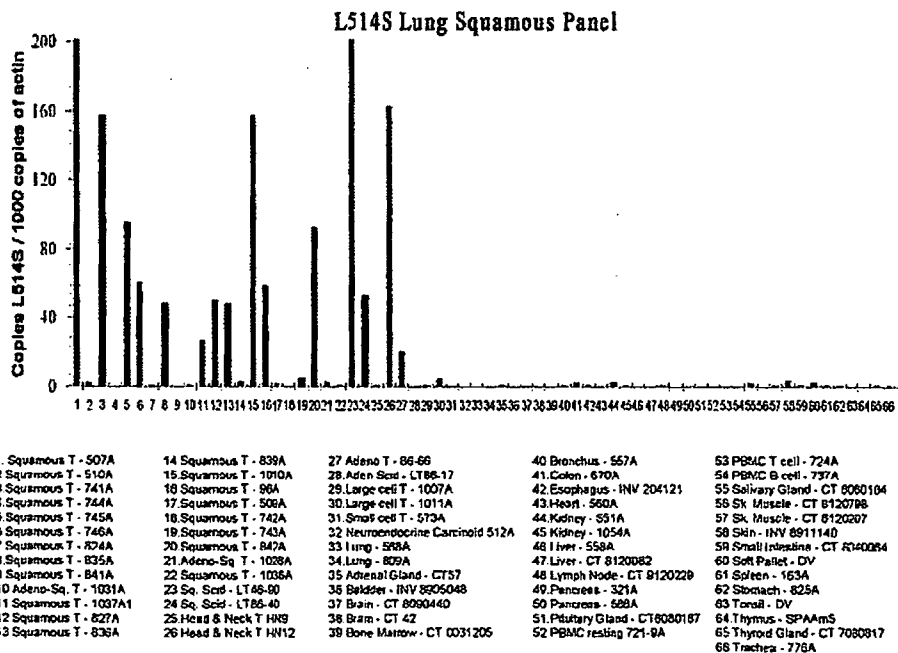
Comparison of patient Ab titers for the three CT antigens

From the 130 USA patients' specimens and the 48 normal donors' sera tested, 6 patients' pleural effusions, 5 patients' sera, and 1 normal donor's serum were selected as representative samples and analysed further to determine the Ab titers towards L514S, L552S, and NY-ESO-1. As shown in Figure 3 (A and B, middle panels), Abs specific to L552S could be detected in

Table 1

L514S, L552S and NY-ESO-1 expression in non-small cell lung tumors.

NSCLC Tumor Specimens	CT Antigen Expression		
	L514S	L552S	NY-ESO-1
All	19·40 (48%)	16·40 (40%)	3·25 (12%)
Adenocarcinoma	8·20 (40%)	12·20 (60%)	3·25 (12%)
Squamous cell carcinoma	11·20 (55%)	4·20 (20%)	-

Figure 1

L514S Lung Squamous Panel

| I. Squamous T - 507A	14 Squamous T - 839A	27 Adeno T - 86-66	40 Bronchus - 557A	53 PBMC T cell - 724A
2 Squamous T - 510A	15 Squamous T - 1010A	28 Aden Scid - LT86-17	41 Colon - 670A	54 PBMC B cell - 737A
3 Squamous T - 741A	16 Squamous T - 96A	29 Large cell T - 1007A	42 Esophagus - INV 204121	55 Salivary Gland - CT 6060104
4 Squamous T - 744A	17 Squamous T - 509A	30 Large cell T - 1011A	43 Heart - 560A	56 Sk Muscle - CT 8120798
5 Squamous T - 745A	18 Squamous T - 742A	31 Small cell T - 573A	44 Kidney - 551A	57 Sk Muscle - CT 8120207
6 Squamous T - 746A	19 Squamous T - 743A	32 Neuroendocrine Carcinoid 512A	45 Kidney - 1054A	58 Skin - INV 8911140
7 Squamous T - 574A	20 Squamous T - 847A	33 Lung - 568A	46 Liver - 558A	59 Small Intestine - CT 8040064
8 Squamous T - 835A	21 Adeno-Sq T - 1028A	34 Lung - 809A	47 Liver - CT 8120082	60 Soft Pallet - DV
9 Squamous T - 841A	22 Squamous T - 1036A	35 Adrenal Gland - CT57	48 Lymph Node - CT 9120229	61 Spleen - 163A
10 Adeno-Sq. T - 1031A	23 Sq. Scid - LT46-90	36 Bladder - INV 8905048	49 Pancreas - 321A	62 Stomach - 825A
11 Squamous T - 1037A1	24 Sq. Scid - LT86-40	37 Brain - CT 8090440	50 Pancreas - 568A	63 Tonsil - DV
12 Squamous T - 827A	25 Head & Neck T HN9	38 Brain - CT 42	51 Pituitary Gland - CT6080167	64 Thymus - SPAAmS
13 Squamous T - 836A	26 Head & Neck T HN12	39 Bone Marrow - CT 0031205	52 PBMC resting 721-9A	65 Thyroid Gland - CT 7080817
				66 Trachea - 776A

Real-time PCR analysis of L514S expression in lung squamous tumors. A panel of 66 cDNA samples composed of 32 tumor specimens and 34 normal tissues was tested. L514S mRNA expression was analyzed by real-time PCR. Overexpression was defined as >10-fold expression as compared to the highest expression in normal tissue except for testis. L514S was overexpressed in 11 of 20 lung squamous tumors.

www.cancerimmunity.org

432

pleural effusions (LPE 298-19 and G361) diluted 10^4-fold and in sera (serum LB3-109) diluted 10^5-fold. The titers were similar to those of the NY-ESO-1-specific Abs in specimen LPE 574-57, even though some pleural effusions, such as LPE 659-29, have a lower titer of L552S-specific Abs (Figure 3A, middle panel). These data clearly show that L552S-specific Ab responses were induced in NSCLC patients at a level similar to that seen against NY-ESO-1.

In the case of L514S (Figure 3, left panels), specific Ab responses were detected in pleural effusions (LPE 659-23, LPE 298-19, and LPE G244) diluted approximately 10^3- to 10^4-fold,

similar to or slightly lower than the titer of NY-ESO-1-specific Abs of LPE 574-57. However, the titers of L514S-specific Abs in sera (L133, L152, and L175) were significantly lower than those of L552S- and NY-ESO-1-specific Abs in sera. It has been suggested that only advanced stage cancer patients have higher titers of L514S-specific Abs because all of these effusion samples were from stage IV patients. Moreover, it was observed that the specific Abs detected to the three CT antigens were of the IgG1 and IgG3 class, suggesting that these humoral responses have been class-switched with T cell help.

Figure 2
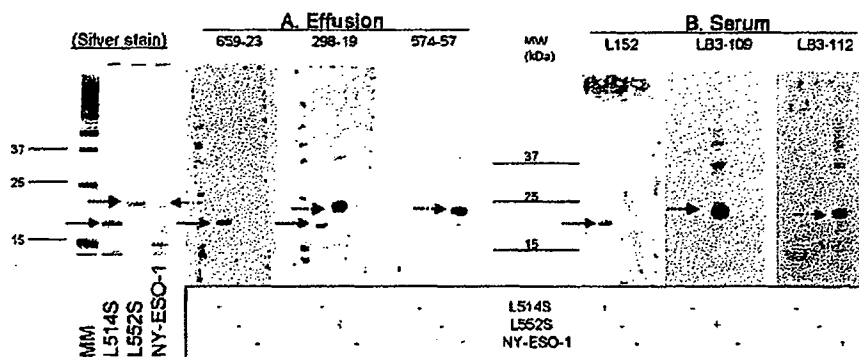
Western blot analysis of NSCLC patients' pleural effusions and sera for Abs against L514S, L552S, and NY-ESO-1. Three pleural effusions (A) and three sera (B) were selected by ELISA using His-tag recombinant proteins L514S (solid arrow), L552S (dotted arrow), and NY-ESO-1 (partially dotted arrow). These were added to a nitrocellulose membrane on which the three proteins were blotted. After washing with 0.05% Tween/PBS, the membranes were developed by HRP-conjugated antihuman IgG and chemiluminescence substrate. The molecular weights of the L514S, L552S, and NY-ESO-1 His-tag proteins were determined to be 16 kDa, 18 kDa, and 18 kDa, respectively, by silver staining (left).

Figure 3
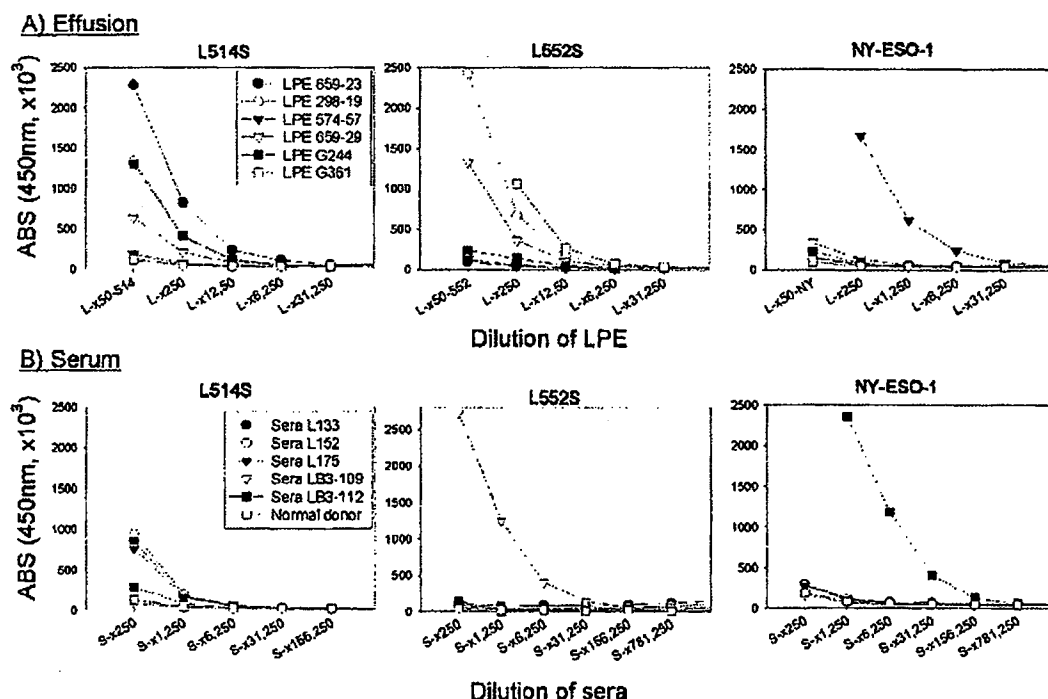
Titration analysis of L514S-, L552S-, and NY-ESO-1-specific Abs in pleural effusions and sera of NSCLC patients. Patients' pleural effusions (A) were diluted 50- to 31,250-fold, and sera (B) were diluted 250- to 781,250-fold with PBS containing 5% goat serum and 5% non-fat dry milk (NFDM). The samples were incubated in 96-well plates that had been protein-coated and blocked with 10% NFDM/PBS. After washing with 0.05% Tween/PBS, the plates were developed by HRP-conjugated antihuman IgG and substrate.

433

Incidence of Abs specific to L514S, L552S, or NY-ESO-1 in NSCLC patients in the USA and Japan

Next, we screened the sera of 90 and 60 NSCLC patients from the USA and Japan, respectively, in order to determine if these CT antigens were recognized by Abs from patients in the two countries in a similar manner. The sera of USA patients were analyzed by ELISA and confirmed by Western blot analysis (300-fold dilution); sera of Japanese patients were analyzed by ELISA and classified into two groups, low titer (>100-fold dilution) and high titer (>10⁴-fold dilution). As shown in Table 2, Abs specific to NY-ESO-1 were detected in 3.3% and 8.3% of the sera of NSCLC patients in the USA and Japan, respectively. The frequency of Abs specific to the other two CT antigens assayed

was high, as much as 12-14% for L514S and 12-23% for L552S in USA and Japanese patients. In contrast, the 48 normal donors assayed did not have any Abs specific to the three CT antigens tested. The absence of NY-ESO-1-specific Abs in normal donors was consistent with an earlier report (20). Moreover, high titers of L552S-specific Abs were also observed in Japanese patients, as high (> 10⁴-fold dilution) as those seen for NY-ESO-1-specific Abs; however, only low titers of L514S-specific Abs were observed in this study. Thus far, we have not found any significant ethnic differences in the rates of Abs specific for these three CT antigens, even though L552S- and NY-ESO-1-specific Abs were relatively more frequent in Japanese patients than in patients from the USA. More importantly, it was found that

Table 2

Frequency of Abs against L514S, L552S and NY-ESO-1 in the sera of stage I-IV NSCLC patients from the US and Japan

Study Group	Country	Specimens	Frequency of Abs against CT Antigen		
			L514S	L552S	NY-ESO-1
NSCLC patients	US	sera	13/90 (14%)	11/90 (12%)	3/90 (3.3%)
	Japan	sera (low titer, >x10²)	7/60	10/60	1/60
		sera (high titer, >x10⁴)	0/60	4/60	4/60
		total	7/60 (12%)	14/60 (23%)	5/60 (8.3%)
	US + Japan	total	20/150 (13%)	25/150 (17%)	8/150 (5.3%)
Normal volunteers	US	sera	0/48 (0%)	0/48 (0%)	0/48 (0%)

Figure 4
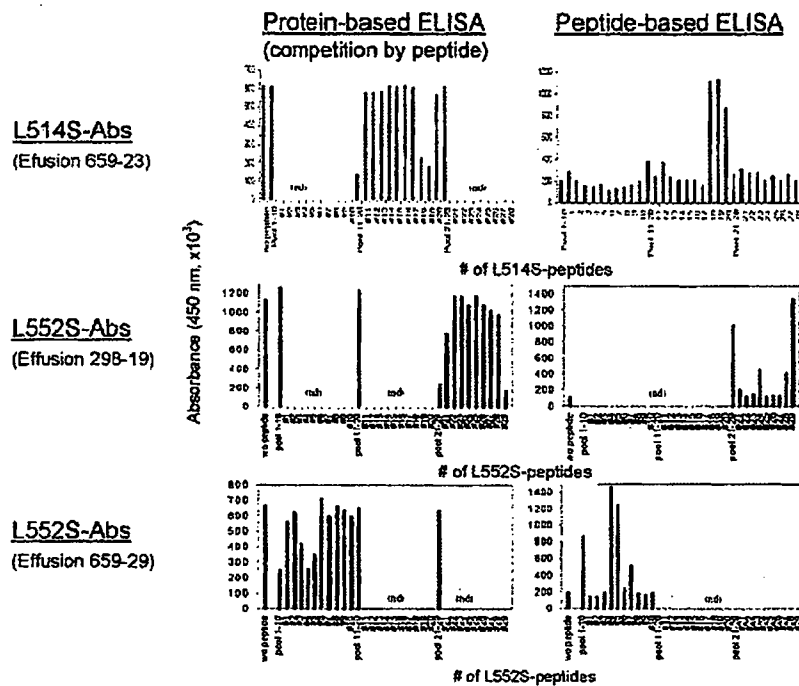
Epitope analysis of L514S- and L552S-specific Abs in NSCLC patients. For the competitive ELISA (left panels), plates were coated with L514S (upper left panel) or L552S (middle and lower left panels) protein and blocked with 10% NFDM/PBS. Diluted (300x) pleural effusion, with or without pooled or individual peptides of L514S or L552S, was then added to the plates. For the peptide-based ELISA (right panels), pooled and individual peptides of L514S (upper right panel) or L552S (middle and lower right panels) were coated on 96-well plates. After the plates were blocked with 10% NFDM/PBS, diluted (300x) patients' PEs were added. After washing, both plates were developed with HRP-conjugated antihuman IgG and substrate.

Figure 5
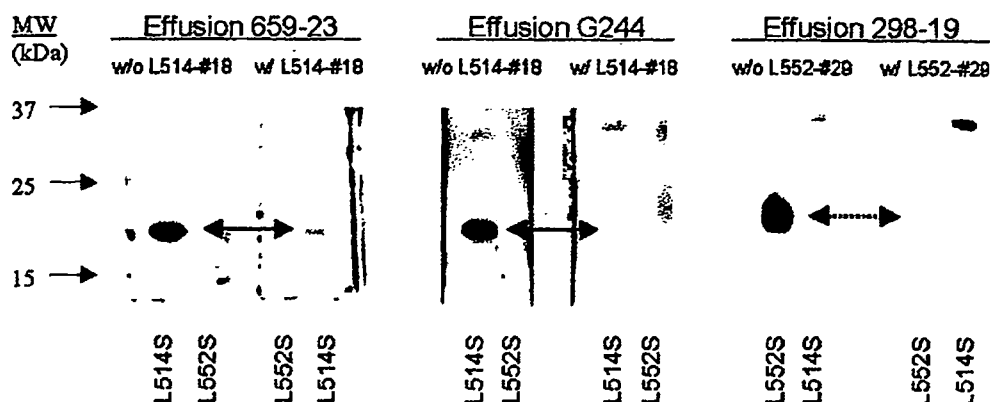
Competitive Western blot analysis with epitopic peptides of L514S and L552S. Patient pleural effusions (300-fold dilution: 659-23, G244, and 298-19) were incubated 30 min in the absence (left) or presence (right) of L514S peptide #18 or L552S peptide #29 at a concentration of 10 µg/ml. They were then assessed by Western blot analysis.

30% or more of the NSCLC patients studied had generated Ab responses specific to one of the three CT antigens evaluated.

Epitope analysis of L514S- and L552S-specific Abs

In order to characterize the Abs specific to these CT antigens, we set up experiments using peptides to identify the epitopes recognized by the L514S- and L552S-specific Abs in the patients' specimens. The ELISA plate was coated with L552S or L514S protein, and patient Abs and peptides 20-aa in length derived from these CT antigens were added simultaneously to see how they competed for Ab recognition (protein-based ELISA). In parallel, 20-aa peptides covering the entire L514S and L552S molecules and overlapping by 15 aa were also utilized for the peptide-based ELISA to see whether patient Abs bound to the individual peptides. As shown in Figure 4 (protein-based ELISA, left panels), peptide pool #11-20 of L514S blocked the binding of Abs in pleural effusion 659-23 to L514S-protein, but peptide pools #1-10 and #21-28 did not block Ab binding to L514S-protein. This competition by a peptide pool was also observed with pleural effusion G244 (data not shown), in which the same peptide pool (#11-20) blocked the binding of Abs to L514S protein. Further breakdown into individual peptides showed that L514S peptides #18 and #19 included the major L514S-specific Ab epitope in pleural effusions 659-23 and G244. This was further demonstrated by the pooled or individual peptide-based ELISA. Namely, peptides #18 and #19, coated on ELISA plates were recognized by L514S-specific Abs in pleural effusion 659-23 (Figure 4, upper right panel). L514S-specific Abs in pleural effusion G244 also mainly recognized peptides #18 and #19 coated on ELISA plates (data not shown). Both the protein-based and the peptide-based ELISAs clearly showed that L514S peptides #18 and #19 include the common epitope recognized by multiple patients' L514S-specific Abs. Thus far, all the patients' Abs specific to L514S protein tested recognized peptides #18/#19 as the major epitope. Interestingly, rabbit Abs generated by immunization with the L514S protein also recognized peptides #18/#19 (data not shown).

In the case of L552S (Figure 4, middle and lower left panels), peptide pool #21-29 of L552S blocked Ab binding to L552S

protein in pleural effusion 298-19, but peptide pools #1-10 and #11-20 did not block Ab binding to L552S protein. In contrast, peptide pool #1-10 blocked pleural effusion 659-29, but other peptide pools did not. Further breakdown into individual peptides showed that the C-terminal peptide #29 is the major epitope of L552-specific Abs in pleural effusion 298-19, and peptides #4 and #5 include the major epitope of L552S-specific Abs in pleural effusion 659-29. The peptide-based ELISA of L552S further confirmed these findings. As shown in Figure 4 (middle and lower right panels), peptide #29 included the epitope of L552S-specific Abs in pleural effusion 298-19, and peptides #4 and #5 included the epitope of the patients' L552S-specific Abs. Both the competitive analysis and the peptide-based ELISA clearly showed that peptides #4/#5 and peptide #29 included the epitope of L552S-specific Abs in the patients' pleural effusions. Interestingly, the major epitopes of rabbit Abs induced by immunization with the L552S protein were present in the C-terminal end #29 peptide of L552S. The minor epitopes localized to the N-terminal of L552S (data not shown).

These data were confirmed by Western blot analysis. As shown in Figure 5, the recognition of L514S protein by pleural effusion 659-23 was largely, but not completely, blocked by the addition of peptide #18 (10 µg/ml). The recognition of L514S protein by Abs in pleural effusion G244 was completely blocked by the addition of peptide #18 at a concentration of 10 µg/ml. For L552S, the specific recognition of pleural effusion 298-19 was completely blocked by the addition of peptide #29 (10 µg/ml). These data were identical in both types of ELISA. These data also suggest that the Abs specific to L514S and L552S are already skewed to recognize one major epitope of L514S and L552S.

Sequence homology to the epitopes defined

We searched for amino acid sequences homologous to that of the epitopes identified in order to explain the Ab specificity to L514S and L552S. A search of the Entrez protein database showed that the amino acid sequence overlapping peptides #18 and #19 of L514S (aa 86-100; RDAKITPEAFEKLGF) was found in L514S but not in other molecules. The amino acid sequence overlapping peptides #4 and #5 of L552S (aa 16-30;